Multipolar Engineering of Subwavelength Dielectric Particles for Scattering Enhancement

S. Krasikov,[1] M. Odit,[1,2] D. Dobrykh,[1,3] I. Yusupov,[1] A. Mikhailovskaya,[1,3] D. Shakirova,[1] A. Shcherbakov,[1] A. Slobozhanyuk,[1] P. Ginzburg,[3,4] D. Filonov,[4] and A. Bogdanov[1,*]

[1] *Department of Physics and Engineering, ITMO University, St. Petersburg, 197101, Russia*

[2] *Electrotechnical University LETI, St. Petersburg, 197376, Russia*

[3] *School of Electrical Engineering, Tel Aviv University, 69978 Tel Aviv, Israel*

[4] *Center for Photonics and 2D Materials, Moscow Institute of Physics and Technology, Dolgoprudny, 141700, Russia*

(Received 25 August 2020; revised 7 November 2020; accepted 4 January 2021; published 22 February 2021)

Electromagnetic scattering on subwavelength structures is attracting much attention owing to the broad range of possible applications where this phenomenon can be used. Fundamental limits of the scattering cross section, which are well understood in spherical geometries, are overlooked in cases of low-symmetry resonators. Here we revise the notion of superscattering and link this property with symmetry groups of scattering potentials. We demonstrate pathways to spectrally overlap several eigenmodes of a resonator in a way such that they interfere constructively and increase the scattering cross section. As a particular example, we demonstrate spectral overlapping of several electric and magnetic modes in a subwavelength ceramic resonator. The optimized structures have a dipolar scattering cross-section limit exceeding that for a sphere by up to a factor of 4. The revealed rules, which link symmetry groups with fundamental scattering limits, allow assessment of the designs and performance of subwavelength superscatterers, which can be used in label-free imaging, compact antennas, long-range radio-frequency identification, and many other fields.

DOI: 10.1103/PhysRevApplied.15.024052

I. INTRODUCTION

Interaction of the electromagnetic waves with matter has been a subject of intensive fundamental and applied studies over the years. Since Maxwell's equations were proven to describe classical phenomena in a closed form, research efforts shifted toward more applied directions. Scattering is a phenomenon with a far-reaching practical applications, ranging from molecular spectroscopy to wireless power transfer and wireless communications [1–7]. Thus, efficient manipulation of electromagnetic scattering underlies antenna devices, radars, and radio-frequency-identification technologies. A long-standing challenge in the field remains the miniaturization of resonating elements without significant degradation of their performance. Typically, the scattering cross section (SCS) of a massive object is directly linked to its geometrical size, unless resonant phenomena are involved [8]. It might be quite counterintuitive that the SCS of subwavelength lossless structures does not depend on their sizes if the resonance condition is maintained. The latter can be achieved by using a plasmonic resonance, increasing the refractive index of particles while reducing their sizes, or loading the antennas with additional impedances [9–14]. These approaches are applied in the field of all-dielectric nanophotonics or gigahertz-range metamaterials. What is affected by the resonator size is the scattering peak bandwidth, which drops significantly with the form factor—this is the Chu-Harrington limit [15,16]. Since the introduction of the concept, quite a few additional fundamental bounds (e.g., Geyi's limit) have been derived [17]. It is clear that a significant SCS enhancement in subwavelength geometries can be achieved only with spectral colocation of several resonances. This approach is directly linked to the topic of superdirective antennas, the pros and cons of which are comprehensively covered in a seminal book by Hansen [18].

Analysis of fundamental scattering bounds is well understood in application to spherically symmetric scatters [8]. In this case, the far-field signatures are directly mapped on eigenmodes of a structure. The scattered field can be expanded into a series of vector spherical harmonics, forming an orthogonal basis for the vector field in three-dimensional space. Each harmonic has a characteristic far-field radiation pattern associated with the far

*a.bogdanov@metalab.ifmo.ru

field of a point multipole (dipole, quadrupole, octupole, etc.) [19]. Thus, vector spherical harmonics are often called "multipoles." Because of orthogonality, each multipole represents an independent scattering channel, and thus the total SCS (C_{SCT}) can be written as the sum of partial cross sections: $C_{\mathrm{SCT}} = \sum_{\ell,m,\sigma} C^{\sigma}_{\ell m}$, where ℓ is the orbital angular momentum and m is its projection on an arbitrarily chosen z axis and it is subject to $-\ell \leq m \leq \ell$, and σ labels polarization. For spherically symmetric resonators, each partial cross section has an upper bound C^{ℓ}_{max} (single-channel limit), which depends only on the wavelength λ and angular momentum ℓ [20,21]:

$$C^{\ell}_{\mathrm{max}} = \frac{2\ell+1}{2\pi}\lambda^2. \tag{1}$$

The scattering cross section reaches this limit at the corresponding Mie-resonance. To surpass this single-channel limit, several Mie resonances should be spectrally overlapped. If this condition is met, a subwavelength structure is considered as a superscatterer [22,23]. Superscattering is usually studied in application to high-symmetry objects, limited to spheres and two-dimensional cylinders [22–28]. The reason is twofold. First, those structures have closed-form analytical solutions, which allows optimal (yet quite complex) conditions for scattering enhancement to be found. Second, each resonance of a sphere corresponds to a single scattering channel as it contributes to a single spherical harmonic. Strictly speaking, the notation of superscattering applies only to the cases when scattering channels [Eq. (1)] can be identified and the overall cross section can be assessed versus the limit [typically the dipolar one ($\ell = 1$) is the most frequently used measure]. If the symmetry of a scatterer is broken, the mapping between multipole expansion and eigenmodes becomes more complicated. In this case, the whole concept of superscattering should be revised since the single-channel limit defined for spherical objects is not valid for nonspherical ones. Different multipoles of the incident field can be scattered into one channel, contrary to the case of high-symmetry resonators, where there is no rescattering between the channels (see Sec. V). Hence, assessing the scattering performances of nonsymmetric structures requires development of the classification tools, paving a way to increase the SCS.

In this work, we investigate the effects of spectral overlapping of Mie resonances, attributed to finite-size symmetric structures, and analyze their impact on scattering enhancement. We generalize the concept of superscattering for finite-size nonspherical objects and derive a fundamental value of a single-channel limit for them. The results are supported by full-wave numerical simulations and experimental measurements in the gigahertz range. In particular, we show that the SCS of a subwavelength finite-height cylindrical resonator can be substantially increased by the colocation of several resonances of different symmetry.

II. GENERALIZATION OF SUPERSCATTERING FOR NONSPHERICAL OBJECTS

The T-matrix method is a semianalytical approach for electromagnetic scattering calculations [29]. The essence of the method is the expansion of both incident and scattered fields into a series of weighted mutually orthogonal vector spherical harmonics. The T matrix links the complex amplitudes within the expansions:

$$\mathbf{b} = \hat{T}\mathbf{a}, \tag{2}$$

where $\mathbf{a}$ and $\mathbf{b}$ are the vectors of complex amplitudes, corresponding to the incident and scattered fields, respectively. Each matrix element $T_{ss'} = \langle s|\hat{T}|s'\rangle$ is the transition amplitude between different multipole channels (from state s to state s'). The indices s and s' encode the polarization (electric or magnetic in respect to a chosen direction), angular momenta ℓ and ℓ', and their projections m and m'. $\hat{T}$ is diagonal in the case of a spherically symmetric scattering potential. This means that each multipole of a spherical resonator is uniquely linked to a single spherical harmonic (multipole). Thus, there is no coupling between different multipoles and, for example, a dipole harmonic of the incident field can be scattered only into the dipole channel. It is worth highlighting that true eigenmodes of a structure cannot be one-to-one mapped to the scattering channels even for a spherical resonator. The reason is that different modes can have the same radiation pattern and thus cannot be orthogonal in the far field. Therefore, a natural set of scattering channels is formed by vector spherical functions but not by eigenmodes of the resonator.

However, for nonspherical resonators, the multipoles contributing to the scattered field are partially mixed, but still form independent (nonintersecting) sets. Those sets can be linked via the eigenmodes of a scatterer, which can be classified with different symmetry groups. By rearrangement of multipole indices, the T matrix of a nonspherical resonator can be presented in a block-diagonal form [30]:

$$\hat{T} = \mathrm{diag}\{\hat{T}_1, \hat{T}_2, \ldots\}, \tag{3}$$

where the blocks $\hat{T}_s$ correspond to the modes of different symmetry. The T matrix of a nonspherical scatterer made of homogeneous isotropic material can be calculated rigorously by the extended-boundary-condition method proposed by Waterman [31]. Two eigenmodes are affiliated with two different blocks if they are transformed differently under the operations of the resonator's symmetry group. The mixing rules and therefore the multipoles entering a certain block are defined by their transformation properties. Depending on the symmetry of the resonator, the number of blocks can be either infinite or finite [32]. If the resonator's group symmetry contains a rotation axis of infinite order (a body of revolution, e.g., sphere, cylinder,

cone, or two-sphere dimer), then the number of the blocks is infinite. In all other cases, the number is finite. The T matrix, reduced to the block diagonal form, can be easily inverted. This property is extremely important for performing efficient numerical routines aimed at solving scattering problems [33].

Applying group-theory approaches, one may say that the multipoles contributing to the same block of $\hat{T}$ form an orthogonal basis of the irreducible representation (irrep) of the resonator's symmetry group [30]. The number of blocks is equal to the number of classes of the symmetry group or, in other words, the number of its irreducible representations [34]. Indeed, it is known in group theory that there is a one-to-one correspondence between the different mode types and irreducible representations (the Wigner theorem) [35]. Therefore, the independent scattering channels of low-symmetry structures are associated with irreducible representations but not with particular multipoles as in the case of spherical resonators. Thus, the total SCS can be represented as a sum of partial SCSs corresponding to the different irreducible representations:

$$C_{\mathrm{SCT}} = \sum_{s=\mathrm{irreps}} \sum_{\ell,m,\sigma} C_{\ell m}^{\sigma s}. \tag{4}$$

Of course, this equation is also valid for spherical resonators, where the polarization σ and angular momentum ℓ identify the irreducible representations of $O(3)$—the group of rotations in three dimensions [36]. The number of irreducible representations is finite for most point-symmetry groups, and thus we have a finite number of independent scattering channels. An exception as we mentioned above is resonators with a rotation axis of infinite order. Therefore, we can conclude that to achieve superscattering for a nonspherical resonator, we need to provide coincidence of resonant frequencies for several modes from different irreducible representations (different blocks of the T matrix). This is possible by tuning the geometry of the resonator and preserving its symmetry. Figure 1 illustrates the relation between scattering channels corresponding to multipoles, irreducible representations of the resonator's symmetry group, and blocks of the T matrix by the example of a cylindrical resonator. Here a_i and b_i are the complex amplitudes of the incident and scattered fields. The insets show the characteristic mode profiles of the cylindrical resonator. E_{1u} and A_{2g} are the standard notation of irreducible representations. Therefore, to have superscattering for nonspherical resonator, two or more resonances corresponding to the eigenmodes from different blocks of the T matrix should be tuned to the same frequency.

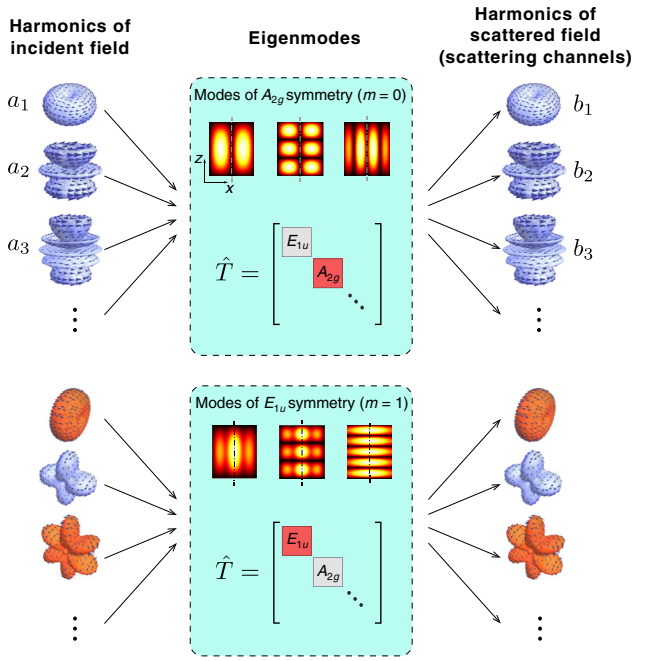

FIG. 1. Relation between scattering channels corresponding to multipoles, irreducible representations of the resonator's symmetry group, and blocks of the T matrix by the example of cylindrical resonators. Here a_i and b_i are the complex amplitudes of the incident and scattered fields. The colormaps show the characteristic mode profiles of the cylindrical resonator.

III. MAXIMIZATION OF THE SCATTERING CROSS SECTION FOR A CYLINDRICAL RESONATOR

A. Numerical optimization

To show that the SCS can be increased by the spectral overlapping of the modes from different irreducible representations, we consider a finite-size cylindrical resonator made of homogeneous dielectric material with permittivity $\varepsilon_{\mathrm{cyl}}$. The resonator is illuminated by a TE-polarized incident wave, as shown in Fig. 2(a). The further results are general and applicable for a wide range of permittivities $\varepsilon_{\mathrm{cyl}}$ and wavelengths λ but to be specific and have an illustrative example we assume that the cylinder is made of high-refractive-index ceramics with $\varepsilon_{\mathrm{cyl}} = 44.8$ and loss tangent $\tan\delta = 10^{-4}$. Such materials demonstrate pronounced Mie resonances [8,37,38] and they are quite useful for compact filters, antennas, wireless power-transfer systems, and radio-frequency-identification technologies [6,39–43].

The calculations of the SCS spectra for different values of the aspect ratio are done with the T-matrix method and then verified by full-wave numerical simulation using CST Microwave Studio and COMSOL Multiphysics [29,44]. The numerical results are shown in Fig. 3(a), where the values of C_{SCT} are normalized to the dipolar single channel

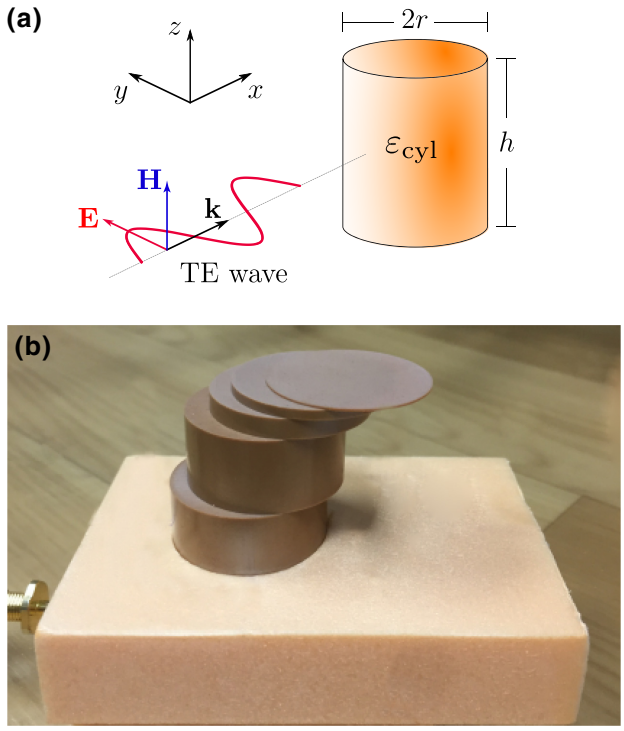

FIG. 2. (a) Geometry of the system under consideration—a TE-polarized plane wave scattered by a dielectric cylinder of height h and radius r. (b) Experimental sample consisting of several ceramic cylinders with different heights and the same radius of 15.7 mm. The dielectric permittivity of the sample $\varepsilon_{cyl} = 44.8$ and the loss tangent $\tan\delta = 10^{-4}$.

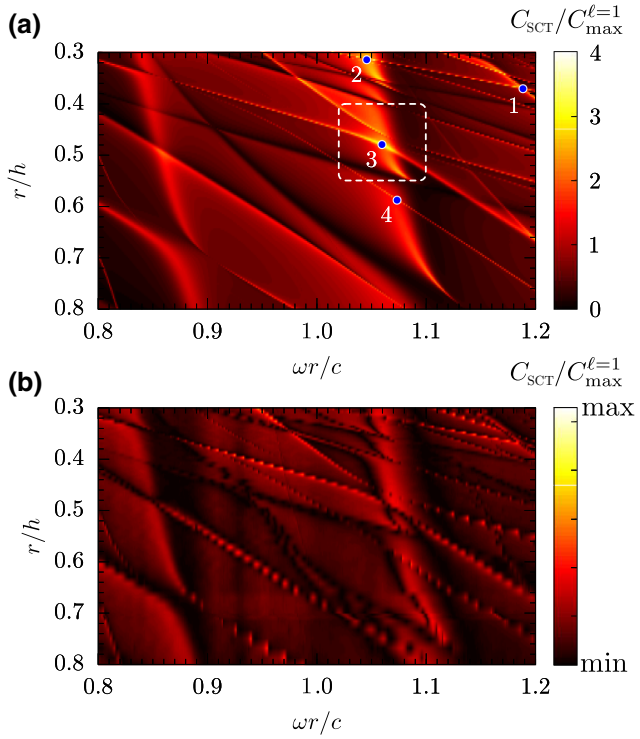

FIG. 3. Color maps of the total scattering cross section as a function of the normalized frequency $\omega r/c$ and the cylinder's aspect ratio r/h. Cross sections are normalized to the corresponding dipole single-channel limit [Eq. (1)]. The cylinder's permittivity $\varepsilon_{cyl} = 44.8$ and the loss tangent $\tan\delta = 10^{-4}$. The incident wave is TE polarized [see Fig. 2(a)]. (a) Numerical calculations. Blue dots (1–4) indicate the highest values of the normalized scattering cross section. The dashed white rectangle indicates the area around the most-pronounced maximum. (b) The experimental scattering-cross-section spectra.

[Eq. (1), $\ell = 1$] to highlight the relative increase. The incident wave is TE polarized [the electric field is perpendicular to the cylinder's axis, see Fig. 2(a)].

The color map in Fig. 3(a) demonstrates the impact of resonant modes on the SCS. The bright branches indicate the evolution of modes as a function of the system's parameters. For example, increasing the aspect ratio of the cylinder leads to reduction of the resonant frequencies of its basic electric and magnetic modes. The most interesting points on the color map are those where several modes of the cylinder are overlapped. Four typical points, marked in the plot, are chosen for a detailed analysis, and the system's parameters for those cases are summarized in Table I. It can be seen that the SCS exceeds the single-channel dipolar limit for spherical objects by a factor of 3-4 if the parameters are properly adjusted.

It is important to highlight that the proposed design is very simple and practical as the scattering enhancement is achieved by tuning of only one geometrical parameter without a need to use coating layers or additional structuring of the resonator's surface as in Refs. [24–28].

B. Sample and experimental measurements

We now provide an experimental verification of the scattering enhancement in the gigahertz frequency range. To vary the height of the cylindrical resonator, we slice a long ceramic rod into several sections and obtain a collection of ceramic disks with different heights and an identical radius (15.7 mm). The rod is manufactured by the sintering of ceramic powder of $LaAlO_3$-$CaTiO_3$ into a solid. The permittivity of the fabricated disks $\varepsilon_{cyl} = 44.8$ and the loss tangent $\tan\delta = 10^{-4}$ for low gigahertz frequencies [45]. The fabricated set of the polished disks allows us

TABLE I. Maximal values of the scattering cross section.

Point	$C_{SCT}/C_{max}^{\ell=1}$	r/h	$\omega r/c$
1	4.01	0.369	1.187
2	3.93	0.312	1.044
3	3.36	0.480	1.062
4	2.75	0.582	1.073

to change the heights in the range from 0.25 to 15 mm with a step of 0.2 mm. Figure 2(b) shows several representative examples. A dielectric foam holder is fabricated by drilling Penoplex—a foam material transparent to gigahertz waves.

The SCSs of the structures are measured in an anechoic chamber. Wideband horn antennas (operational range 1–18 GHz) are connected to ports of Agilent E8362C vector network analyzer. Transmitting antenna excite a quasiplane wave impinging the resonator placed in the far-field zone. The incident field is TE polarized. The scattered field in the forward direction is collected with an additional horn antenna, which is connected to the second port of the vector network analyzer. The background signal, obtained from the measurements without a sample present, is subtracted [46]. Additionally, the time-gating technique is applied to reduce residual reflections from the horn antennas and setup elements [47]. The measured complex transmission coefficient is used to calculate the total SCS via the optical theorem [48,49]. Figure 3(b) shows the measured map of the SCS. The high quality of the samples and accurate experimental acquisition provide a very good agreement between the numerical and experimental data, clearly demonstrating the mode intersection at points where the SCS is maximal.

IV. MODAL AND MULTIPOLE DESCRIPTION OF SCATTERING ENHANCEMENT

To show that the scattering enhancement [points 1, 2, 3, and 4 in Fig. 3(a)] is directly related to the overlapping of the eigenmodes transforming under different irreducible representations, we calculate the eigenmode spectrum as a function of the aspect ratio [see Fig. 4(a)]. These calculations are performed with COMSOL Multiphysics. To get only the modes that can be excited by a plane TE-polarized wave [see Fig. 2(a)], we perform the simulation in a quarter of space applying a perfect-electric-boundary condition to the x-z plane and a perfect-magnetic-boundary condition to the x-y plane. To classify the modes, we analyze their transformation rules using the character tables for point symmetry group $D_{\infty h}$—the symmetry group of a finite cylinder [50,51]. The modes of a finite cylinder can be characterized by the azimuthal number $m = 0, 1, 2, \ldots$ and parity (odd or even) of the electric field distribution with respect to the mirror reflection $z \to -z$. For $m = 0$ we can introduce the polarization of the mode (TE or TM). It is worth mentioning that an orbital number ℓ is not a good quantum number of the mode as it is in the case of spherical resonators. The classification of the modes in a finite cylinder and their connection to the irreducible representations of $D_{\infty h}$ are shown in Table II. The first column shows the notation of irreducible representations; the second column shows the azimuthal numbers—projections of angular momentum on the z axis; the third column shows the polarization of the mode (in the cases when it can be defined); the fourth column shows the parity of the mode (odd or even) under its reflection in the x-y plane; the last column indicates whether it is possible to excite the mode by the TE-polarized wave propagating perpendicular to the cylinder axis. A characteristic electric field distribution and the multipole content for several modes from different irreducible representations are shown in Fig. 4(d). The detailed mode classification and multipole analysis in the resonators of different symmetry groups is provided in Ref. [52].

The modes from different irreducible representations are shown in Fig. 4(a) with different colors. We use the standard notation of the irreducible representations [53]. One can see that only the modes from different irreducible representations can intersect, producing a crossing in the parametric space. The modes from the same irreducible representation repel each other, forming an avoid crossing [see modes A_{2g} in Fig. 4(a)]. In quantum mechanics, this fact is well known as the von Neumann–Wigner theorem [35]. This repulsion is a common feature of open systems [54] and it is explained by the interaction of the modes through the continuum of propagating waves in the surrounding space. In particular, high-Q quasi-bound states in the continuum can appear as a result of this interaction [44,55–57].

As an example, we investigate the scattering enhancement near point 3 in Fig. 3(a) in more detail. By comparing the spectral position of the maximum of the SCS in Figs. 3(a) and 4(b) with the map of eigenmodes in Fig. 4(a) one can see that the maximum of the SCS appears at $r/h = 0.48$ as a result of the colocation of two modes from different irreducible representations—namely, A_{2g} and E_{1u}. The maximal value of the SCS in this case exceeds the dipolar single-channel limit ($\ell = 1$) for a spherical object by more than 3 times.

Then we can consider the multipole decomposition at the point of the maximal SCS, which can be done with the use of the well-known analytical expression [58]

$$C_{\mathrm{SCT}} = \frac{k^4}{6\pi\varepsilon_0^2|\mathbf{E}_0|^2}\left[\sum_{\alpha}\left(|p_\alpha|^2 + |m_\alpha/c|^2\right) + \frac{1}{120}\sum_{\alpha\beta}\left(|kQ^e_{\alpha\beta}|^2 + \left|\frac{kQ^m_{\alpha\beta}}{c}\right|^2\right) + \frac{1}{315}\sum_{\alpha\beta\gamma}\left(|k^2O^e_{\alpha\beta\gamma}|^2 + \left|\frac{k^2O^m_{\alpha\beta\gamma}}{c}\right|^2\right) + \ldots\right], \tag{5}$$

where $\mathbf{E}_0$ is the amplitude of the incident plane wave, k is the wave number, c is the speed of light in free space, ε_0 is the vacuum permittivity, p_α and m_α are electric and magnetic dipole moments, $Q^e_{\alpha\beta}$ and $Q^m_{\alpha\beta}$ are the electric and magnetic quadrupole moments, and $O^e_{\alpha\beta\gamma}$ and

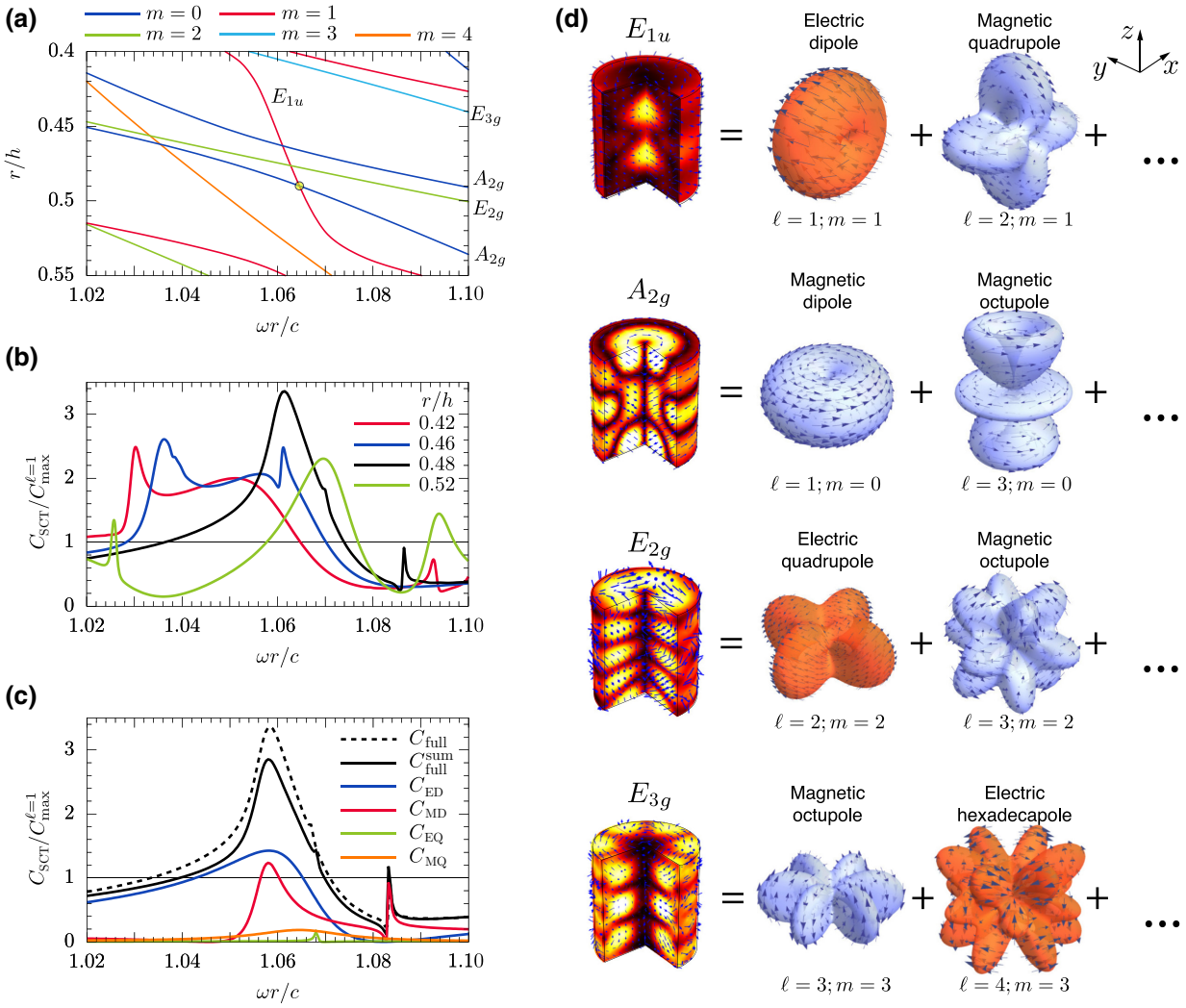

FIG. 4. (a) Spectrum of the eigenmodes calculated in the vicinity of the SCS maxima and their irreducible representations. (b) Spectrum of the SCSs, corresponding to the slices in the diagram in Fig. 3(a). (c) Multipole decomposition of the total SCS at $r/h = 0.48$. The dashed black line corresponds to full-wave numerical simulation and the solid black line is the summation of the partial SCSs [electric dipole (ED), magnetic dipole (MD), electric quadrupole (EQ), and magnetic quadrupole (MQ)] shown by colored lines. (d) Examples of field distributions of eigenmodes corresponding to the irreducible representations considered and their multipole far-field decompositions.

$O^m_{\alpha\beta\gamma}$ are the electric and magnetic octupole moments. The summation indices α, β, and γ run over the Cartesian coordinates x, y, z. These multipole moments can be calculated analytically as volume integrals [59]. The total SCS for subwavelength objects is accurately defined by the lower multipoles. Indeed, it can be seen from Fig. 4(c) that the dominant contribution to SCSs for the modes E_{1u} and A_{2g} is given by the electric and magnetic dipole moments, respectively.

As one can see from Fig. 4(c), the partial SCSs corresponding to the electric and magnetic dipole moments exceed the single-channel limit for a sphere [Eq. (1)]. The reason for this is the mixing of multipoles (see Fig. 1) making possible rescattering between the channels corresponding to different multipoles. Therefore, the single-channel limit should be specified for the case of nonspherical resonators. We discuss it in Sec. V.

According to the optical theorem, when the losses are negligible, the maximization of the SCS should result in an increase of scattering in the forward direction and forward directivity. The directivity in the direction given by the polar and azimuthal angles θ and φ is defined as [8]

$$D(\theta,\varphi) = \frac{4\pi I(\theta,\varphi)}{\int_0^{2\pi}\int_0^{\pi} I(\theta,\varphi)\sin\theta d\theta d\varphi}, \tag{6}$$

where $I(\theta,\varphi)$ is the intensity of the scattered wave in a direction given by θ and φ. Figure 5 shows the directivity patterns in the x-y plane ($\theta = \pi/2$) at points 1, 2, 3, and 4 [see Fig. 3(a)], where the maximal total cross-section is

TABLE II. Irreducible representations of the symmetry group $D_{\infty h}$ and eigenmode classification. m is the azimuthal number. For TM-polarized modes, $\mathbf{E} = (E_\rho, 0, E_z)$ and $\mathbf{H} = (0, H_\varphi, 0)$. For TE-polarized modes, $\mathbf{E} = (0, E_\varphi, 0)$ and $\mathbf{H} = (H_\rho, 0, H_z)$. For even modes, $\mathbf{E}(x, y, -z) = \mathbf{E}(x, y, z)$. For odd modes, $\mathbf{E}(x, y, -z) = -\mathbf{E}(x, y, z)$.

Irrep	m	Polarization of mode	Parity: $z \to -z$	Excitation by TE wave
A_{1u}	0	TM	Odd	No
A_{1g}	0	TM	Even	No
A_{2u}	0	TE	Odd	No
A_{2g}	0	TE	Even	Yes
E_{1g}	1	Hybrid	Odd	No
E_{1u}	1	Hybrid	Even	Yes
E_{2u}	2	Hybrid	Odd	No
E_{2g}	2	Hybrid	Even	Yes
E_{3g}	3	Hybrid	Odd	No
E_{3u}	3	Hybrid	Even	yes
⋮	⋮	⋮	⋮	⋮

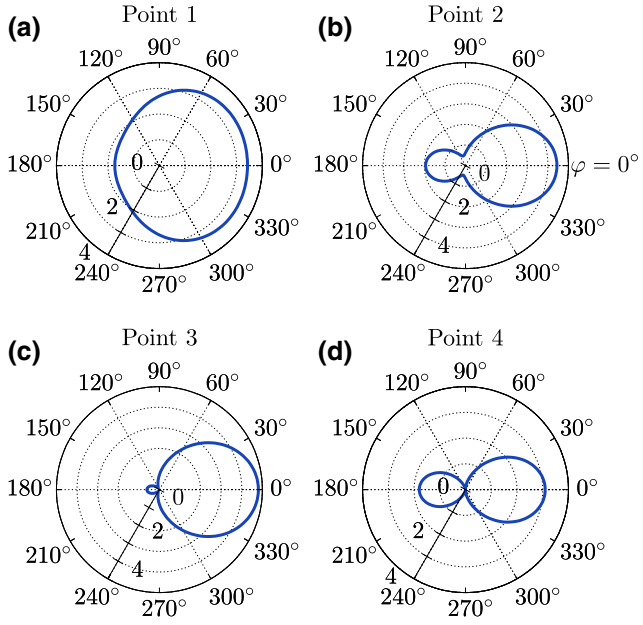

FIG. 5. Directivity patterns obtained for the points corresponding to maximal values of the scattering cross section indicated in Fig. 3(a) and listed in Table I. The forward direction correspond to azimuthal angle $\varphi = 0°$. The scale is linear.

achieved. One can see that for all points the forward directivity exceeds the value of 3 and that for point 3 the forward directivity is almost 5. This fact is quite interesting as it highlights the contribution of relative phases between multipolar contributions, which can constructively interfere and create directive patterns [60,61].

V. DISCUSSION ON THE SINGLE-CHANNEL LIMIT

The single-channel limit, derived for spherical objects [Eq. (1)], is not valid for particles with symmetry of a lower order, as we demonstrated numerically in the previous section. The underlying reason for this inconsistency can be illustrated with the T matrix, which is a relation between the vectors of the complex amplitudes of the incident and scattered waves usually written in the basis of vector spherical harmonics [see Eq. (2)].

In the general case, the T matrix can be written in a block-diagonal form [see Eq. (2)] such that each block T_s corresponds to the modes of certain symmetry, (i.e., from a certain irreducible representation) and the elements of the block are the transition amplitudes between different scattering channels. For example, a quadrupole harmonic from the incident plane wave can be scattered into the dipole channel. This is in a sharp contrast to the case of spherical resonators, where the T matrix is diagonal and therefore there is no rescattering between different channels. This multipole mixing inspired by nonspherical potentials is the reason why the scattering into a single channel can surpass the limit of the same channel for a spherical object.

To generalize the single-channel limit for nonspherical objects we rely on singular-value decomposition [62] and the fact that the SCS cannot exceed the extinction cross section. Following the derivation procedure presented in the Appendix, the upper limit of the partial SCS corresponding to angular momentum ℓ can be determined as

$$C^{\ell}_{\max} = \frac{2\ell + 1}{\pi}\lambda^2, \tag{7}$$

which is only twice as large as the single-channel limit for spherical particles. We emphasize that the question of whether this upper bound can be reached, and, if it can, then under what conditions, remains open and will be the subject of further research. Another important point is that the blocks of the T matrix have an infinite size and therefore the modes contribute to the infinite number of scattering channels. Nevertheless, the SCS remains finite because the contribution of high-order multipoles is negligible for the finite-size objects. Indeed, in practice, the field expansions and the T matrix are terminated at some angular momentum $\ell_{\max}$. If a scatterer is contained within a radius a, then the $\ell_{\max} \approx \omega a/c$ [63,64].

The T-matrix approach formulated in terms of vector spherical harmonics is not a unique method for solving the scattering problem. At first sight, it may seem that a more-natural way is to take a complete set of the eigenfunctions of a resonator as a basis. However, it is well known that for open systems their eigenfunctions (resonant states) diverge at infinity [65,66]. They are not normalized in a regular

way, which makes them less convenient in practice. Nevertheless, having a spectrum of the system and the complete set of resonant states, one can rigorously derive the expression for the scattering matrix of the system or for the total scattering cross section [67–69].

Resonant states cannot be associated with the scattering channels because, for example, two different modes can have the same far-field angular distributions. Therefore, their far fields are not orthogonal and interfere, and the total power scattered by these modes cannot be divided into two independent terms. In contrast, with use of a basis of vector spherical harmonics, the total scattering cross section can be represented as a sum of partial cross sections corresponding to different polarization, orbital momentum, and its projection. Thus, such an approach is more practical and it gives a deeper physical insight into the scattering problem without direct appeal to the eigenmodes.

VI. CONCLUSION

We generalize the concept of superscattering for nonspherical resonators. The main strategy for scattering enhancement is spectral overlapping between eigenmodes of different symmetry. This can be achieved by tuning the geometrical parameters of an object while still preserving its symmetry. The scattering enhancement due to spectral overlap of eigenmodes is demonstrated by the example of a high-index dielectric resonator of finite height, and it is shown to exceed the dipolar single-channel limit for a spherical scatterer by up to a factor of 4. The tuning parameter is the cylinder's aspect ratio, and no coating layers or additional structuring is used. This approach considerably simplifies the design, making it attractive in a broad range of possible applications. The obtained results allow designing compact superscatterers, keeping in mind fundamental limitations that might be faced during the maximization of the performances. We also demonstrate that the partial SCS of a nonspherical object, corresponding to a certain multipole, can exceed the single-channel limit for a sphere for the same multipole. Using singular-value decomposition and the fact that the SCS can notexceed the extinction cross section, we show the single-channel limit for nonspherical objects is twice as large as that for spherical resonators. However, the specific conditions for reaching this limit remains open.

ACKNOWLEDGMENTS

The authors thank Kristina Frizyuk for fruitful discussions and Elizaveta Nenasheva (CEO of Ceramics Co. Ltd.) for sample fabrication. The research was supported by the Russian Science Foundation (Project No. 19-79-10232). A.B. acknowledges the RFBR (Grant No. 19-02-00419) and the BASIS foundation. P.G. acknowledges partial support from ERC StG "In Motion" (Grant No. 802279) and PAZY Foundation (Grant No. 01021248).

APPENDIX: SINGLE-CHANNEL LIMIT FOR NONSPHERICAL SCATTERERS

We derive a general upper limit on a scattering channel of the SCS. The T matrix by definition relates amplitude vectors $\mathbf{a}$ and $\mathbf{b}$ of incident (regular) and scattered (outgoing) fields respectively:

$$\mathbf{b} = \hat{T}\mathbf{a}. \tag{A1}$$

The fact that the scattering power is less than the extinction power leads to the relation (e.g., see Ref. [70], Chapter 6)

$$\mathbf{a}^\dagger \hat{T}^\dagger \hat{T}\mathbf{a} \le -\frac{1}{2}\mathbf{a}^\dagger \left(\hat{T} + \hat{T}^\dagger\right)\mathbf{a} \tag{A2}$$

for any incident field vector $\mathbf{a}$, where the dagger means Hermitian conjugation of a matrix. The equality holds for nonabsorbing particles.

Let us consider singular-value decomposition of the T matrix $\hat{T} = \hat{U}\hat{\Sigma}\hat{V}^\dagger$ with unitary matrices $\hat{U}^\dagger$ and $\hat{V}^\dagger$ (each being composed of a set of orthonormal basis column vectors, $\hat{V} = [\mathbf{v}_1\ \mathbf{v}_2\ \mathbf{v}_3\ \dots]$, $\hat{U} = [\mathbf{u}_1\ \mathbf{u}_2\ \mathbf{u}_3\ \dots]$), and diagonal matrix $\hat{\Sigma}$ of singular values σ_k. Since a can be arbitrary, let us take $\mathbf{a} = \mathbf{v}_k$ in Eq. (A2):

$$\mathbf{v}_k^\dagger \hat{V}\hat{\Sigma}^\dagger \hat{\Sigma}\hat{V}^\dagger \mathbf{v}_k \le -\frac{1}{2}\mathbf{v}_k^\dagger \left(\hat{U}\hat{\Sigma}\hat{V}^\dagger + \hat{V}\hat{\Sigma}^\dagger \hat{U}^\dagger\right)\mathbf{v}_k. \tag{A3}$$

The product $\hat{V}^\dagger \mathbf{v}_k = \mathbf{e}_k$ is the kth column of the unit matrix $\hat{I} = [\mathbf{e}_1\ \mathbf{e}_2\ \mathbf{e}_3\ \dots]$. Then

$$|\sigma_k|^2 \le -\frac{1}{2}\left(\mathbf{v}_k^\dagger \hat{U}\hat{\Sigma}\mathbf{e}_k + \mathbf{e}_k^\dagger \hat{\Sigma}^\dagger \hat{U}^\dagger \mathbf{v}_k\right). \tag{A4}$$

We denote $\hat{W} = \hat{U}^\dagger \hat{V}$, which has the unitary property $\hat{W}^\dagger \hat{W} = \hat{I}$, with kth column $\mathbf{w}_k = \hat{U}^\dagger \mathbf{v}_k$, and then

$$\begin{aligned} |\sigma_k|^2 &\le -\frac{1}{2}\left(\sigma_k \mathbf{w}_k^\dagger \mathbf{e}_k + \sigma_k^* \mathbf{e}_k^\dagger \mathbf{w}_k\right) \\ &= -\mathrm{Re}\left[\sigma_k \left(\mathbf{w}_k^\dagger \mathbf{e}_k\right)\right]. \end{aligned} \tag{A5}$$

For any two complex numbers $z_1 = x_1 + iy_1$ and $z_2 = x_2 + iy_2$

$$|\mathrm{Re}\,(z_1 z_2)| = |x_1 x_2 - y_1 y_2| \le |x_1|\,|x_2| + |y_1|\,|y_2|. \tag{A6}$$

Since $\mathbf{w}_k^\dagger \mathbf{e}_k$ is a projection of $\mathbf{w}_k$, having a unit norm, onto $\mathbf{e}_k$, then $\left|\mathbf{w}_k^\dagger \mathbf{e}_k\right| \le 1$, which means $|x_2| \le 1$, $|y_2| \le 1$ in the latter equation. Thus, the inequality in Eq. (A5) becomes

$$|\sigma_k|^2 \le \left|\mathrm{Re}\left[\sigma_k \left(\mathbf{w}_k^\dagger \mathbf{e}_k\right)\right]\right| \le (|\mathrm{Re}\,\sigma_k| + |\mathrm{Im}\,\sigma_k|). \tag{A7}$$

The latter inequality can be shown to have solutions only when $|\sigma_k|^2 \le 2$. In the case of a spherically symmetric

scatterer, the T matrix is diagonal; hence, $\hat{V}$, $\hat{U}$, and $\hat{W}$ are identity matrices, and the inequality in Eq. (A7) reduces to $|\sigma_k|^2 \leq -\mathrm{Re}\,\sigma_k$ with the solution $|\sigma_k|^2 \leq 1$, which was previously found for the case of Mie scattering on the basis of an analysis of Mie coefficients.

The total averaged scattering power written via the T-matrix singular-value decomposition becomes

$$W_{\mathrm{SCT}} = \frac{\mathbf{a}^\dagger \hat{T}^\dagger \hat{T}\mathbf{a}}{2k^2 Z} = \frac{\mathbf{a}^\dagger \hat{V}\hat{\Sigma}^\dagger \hat{\Sigma}\hat{V}^\dagger \mathbf{a}}{2k^2 Z} = \frac{\tilde{\mathbf{a}}^\dagger \hat{\Sigma}^\dagger \hat{\Sigma}\tilde{\mathbf{a}}}{2k^2 Z} = \frac{1}{2k^2 Z}\sum_{L,\sigma} |\sigma_{L,\sigma}|^2 |\tilde{a}_{L,\sigma}|^2 \leq \frac{1}{k^2 Z}\sum_{L,\sigma} |a_{L,\sigma}|^2, \tag{A8}$$

where $L = (\ell, m)$ is the spherical harmonic index, $Z = \sqrt{\mu_s/\varepsilon_s}$ is the wave impedance of the homogeneous isotropic lossless surrounding medium, $\sigma = e, h$ encodes the polarization of the vector spherical harmonics, and $\tilde{\mathbf{a}} = \hat{V}^\dagger \mathbf{a}$, which means that $|\tilde{\mathbf{a}}|^2 \leq |\mathbf{a}|^2$ since $\hat{V}^\dagger \mathbf{a}$ is the orthogonal subspace projection. Therefore, each partial term in W_{SCT} is bounded by

$$W_{\mathrm{SCT},L,\sigma} \leq \frac{1}{k^2 Z} |a_{L,\sigma}|^2. \tag{A9}$$

In the case of plane-wave incidence along the z axis with a fixed polarization and electric field amplitude E_0,

$$|a_{\ell,m,\sigma}| = \delta_{m,\pm 1}\sqrt{\pi\,(2\ell+1)}E_0, \tag{A10}$$

which yields the partial contribution to the scattering power

$$W_{\mathrm{SCT},\ell,\sigma} \leq \frac{1}{k^2 Z}\sum_{m=\pm 1} |a_{\ell,m,\sigma}|^2 = \frac{2\pi\,(2\ell+1)\,E_0^2}{k^2 Z}. \tag{A11}$$

The corresponding partial contribution to the SCS is

$$C_{\mathrm{SCT},\ell,\sigma} = \frac{W_{\mathrm{SCT},\ell,\sigma}}{\frac{1}{2Z}E_0^2} \leq \frac{(2\ell+1)}{\pi}\lambda^2. \tag{A12}$$

This limit is twice as high as the one for spherical objects.

[1] S. Nie and S. R. Emory, Probing single molecules and single nanoparticles by surface-enhanced raman scattering, Science **275**, 1102 (1997).

[2] K.-S. Lee and M. A. El-Sayed, Dependence of the enhanced optical scattering efficiency relative to that of absorption for gold metal nanorods on aspect ratio, size, end-cap shape, and medium refractive index, J. Phys. Chem. B **109**, 20331 (2005).

[3] J. B. Jackson and N. J. Halas, Surface-enhanced raman scattering on tunable plasmonic nanoparticle substrates, PNAS **101**, 17930 (2004).

[4] J. A. Schuller, T. Taubner, and M. L. Brongersma, Optical antenna thermal emitters, Nat. Photonics **3**, 658 (2009).

[5] L. R. Hirsch, R. J. Stafford, J. A. Bankson, S. R. Sershen, B. Rivera, R. Price, J. D. Hazle, N. J. Halas, and J. L. West, Nanoshell-mediated near-infrared thermal therapy of tumors under magnetic resonance guidance, PNAS **100**, 13549 (2003).

[6] M. Song, P. Belov, and P. Kapitanova, Wireless power transfer inspired by the modern trends in electromagnetics, Appl. Phys. Rev. **4**, 021102 (2017).

[7] J.-M. Geffrin, B. García-Cámara, R. Gómez-Medina, P. Albella, L. Froufe-Pérez, C. Eyraud, A. Litman, R. Vaillon, F. González, and M. Nieto-Vesperinas *et al.*, Magnetic and electric coherence in forward-and back-scattered electromagnetic waves by a single dielectric subwavelength sphere, Nat. Commun. **3**, 1 (2012).

[8] C. F. Bohren and D. R. Huffman, *Absorption and Scattering of Light by Small Particles* (Wiley-VCH, Weinheim, 1998).

[9] S. A. Maier, *Plasmonics: Fundamentals and Applications* (Springer Science & Business Media, New York, 2007).

[10] A. E. Krasnok, A. E. Miroshnichenko, P. A. Belov, and Y. S. Kivshar, All-dielectric optical nanoantennas, Opt. Express **20**, 20599 (2012).

[11] H. Mosallaei and K. Sarabandi, Antenna miniaturization and bandwidth enhancement using a reactive impedance substrate, IEEE Trans. Antennas Propag. **52**, 2403 (2004).

[12] W. E. Liu, Z. N. Chen, X. Qing, J. Shi, and F. H. Lin, Miniaturized wideband metasurface antennas, IEEE Trans. Antennas Propag. **65**, 7345 (2017).

[13] D. Filonov, A. Shmidt, A. Boag, and P. Ginzburg, Artificial localized magnon resonances in subwavelength metaparticles, Appl. Phys. Lett. **113**, 123505 (2018).

[14] D. Dobrykh, A. Mikhailovskaya, P. Ginzburg, and D. Filonov, 4D optically reconfigurable volumetric metamaterials, Phys. Status Solidi (RRL) - Rapid Res. Lett. **14**, 2000159 (2020).

[15] R. F. Harrington, Effect of antenna size on gain, bandwidth, and efficiency, J. Res. Nat. Bur. Stand **64**, 1 (1960).

[16] L. J. Chu, Physical limitations of omni-directional antennas, J. Appl. Phys. **19**, 1163 (1948).

[17] W. Geyi, A method for the evaluation of small antenna q, IEEE Trans. Antennas Propag. **51**, 2124 (2003).

[18] R. C. Hansen, *Electrically Small, Superdirective, and Superconducting Antennas* (Wiley-Interscience, Hoboken, 2006), 1st ed.

[19] A. B. Evlyukhin, T. Fischer, C. Reinhardt, and B. N. Chichkov, Optical theorem and multipole scattering of light by arbitrarily shaped nanoparticles, Phys. Rev. B **94**, 205434 (2016).

[20] C. J. Foot *et al.*, *Atomic Physics* (Oxford University Press, Oxford, 2005), Vol. 7.

[21] M. I. Tribel'skii, Resonant scattering of light by small particles, JETP **86**, 915 (1984).

[22] Z. Ruan and S. Fan, Superscattering of Light from Subwavelength Nanostructures, Phys. Rev. Lett. **105**, 013901 (2010).

[23] Z. Ruan and S. Fan, Design of subwavelength superscattering nanospheres, Appl. Phys. Lett. **98**, 043101 (2011).

[24] C. Qian, X. Lin, Y. Yang, X. Xiong, H. Wang, E. Li, I. Kaminer, B. Zhang, and H. Chen, Experimental Observation of Superscattering, Phys. Rev. Lett. **122**, 063901 (2019).
[25] A. Mirzaei, I. V. Shadrivov, A. E. Miroshnichenko, and Y. S. Kivshar, Cloaking and enhanced scattering of core-shell plasmonic nanowires, Opt. Express **21**, 10454 (2013).
[26] S. H. Raad, C. J. Zapata-Rodríguez, and Z. Atlasbaf, Multi-frequency super-scattering from sub-wavelength graphene-coated nanotubes, JOSA B **36**, 2292 (2019).
[27] C. Qian, X. Lin, Y. Yang, F. Gao, Y. Shen, J. Lopez, I. Kaminer, B. Zhang, E. Li, and M. Soljačić *et al.*, Multi-frequency superscattering from subwavelength hyperbolic structures, ACS Photonics **5**, 1506 (2018).
[28] A. Mirzaei, A. E. Miroshnichenko, I. V. Shadrivov, and Y. S. Kivshar, Superscattering of light optimized by a genetic algorithm, Appl. Phys. Lett. **105**, 011109 (2014).
[29] M. I. Mishchenko, L. D. Travis, and D. W. Mackowski, *T*-matrix computations of light scattering by nonspherical particles: A review, J. Quant. Spectrosc. Radiat. Transfer **55**, 535 (1996).
[30] M. Kahnert, Irreducible representations of finite groups in the *T*-matrix formulation of the electromagnetic scattering problem, JOSA A **22**, 1187 (2005).
[31] P. C. Waterman, Symmetry, unitarity, and geometry in electromagnetic scattering, Phys. Rev. D **3**, 825 (1971).
[32] F. M. Schulz, K. Stamnes, and J. Stamnes, Point-group symmetries in electromagnetic scattering, JOSA A **16**, 853 (1999).
[33] Z. Xiong, Z. Xiong, Q. Yang, Q. Yang, W. Chen, Z. Wang, J. Xu, J. Xu, J. Xu, W. Liu, Y. Chen, Y. Chen, and Y. Chen, On the constraints of electromagnetic multipoles for symmetric scatterers: Eigenmode analysis, Opt. Express **28**, 3073 (2020).
[34] M. Tinkham, *Group Theory and Quantum Mechanics* (Dover Publications, Mineola, N.Y, 2003).
[35] E. P. Wigner, *Group Theory and Its Application to the Quantum Mechanics of Atomic Spectra*, Pure and Applied Physics Vol. 5 (Academic Press, New York, NY, 1959).
[36] D. A. Varshalovich, A. N. Moskalev, and V. K. Khersonskii, *Quantum Theory of Angular Momentum* (World Scientific, Singapore, 1988).
[37] S. Kruk and Y. Kivshar, Functional meta-optics and nanophotonics governed by mie resonances, ACS Photonics **4**, 2638 (2017).
[38] Y. Kivshar and A. Miroshnichenko, Meta-optics with mie resonances, Opt. Photonics News **28**, 24 (2017).
[39] T. Yang, M. Tamura, and T. Itoh, Super compact low-temperature co-fired ceramic bandpass filters using the hybrid resonator, IEEE Trans. Microw. Theory Tech. **58**, 2896 (2010).
[40] D. F. Sievenpiper, D. C. Dawson, M. M. Jacob, T. Kanar, S. Kim, J. Long, and R. G. Quarfoth, Experimental validation of performance limits and design guidelines for small antennas, IEEE Trans. Antennas Propag. **60**, 8 (2011).
[41] Z. Peng, H. Wang, and X. Yao, Dielectric resonator antennas using high permittivity ceramics, Ceram. Int. **30**, 1211 (2004).
[42] D. Dobrykh, I. Yusupov, S. Krasikov, A. Mikhailovskaya, D. Shakirova, A. Bogdanov, A. Slobozhanyuk, D. Filonov, and P. Ginzburg, Long-range miniature ceramic rfid tags, arXiv preprint arXiv:2004.08457 (2020).
[43] M. Song, P. Belov, and P. Kapitanova, Wireless power transfer based on dielectric resonators with colossal permittivity, Appl. Phys. Lett. **109**, 223902 (2016).
[44] A. A. Bogdanov, K. L. Koshelev, P. V. Kapitanova, M. V. Rybin, S. A. Gladyshev, Z. F. Sadrieva, K. B. Samusev, Y. S. Kivshar, and M. F. Limonov, Bound states in the continuum and fano resonances in the strong mode coupling regime, Adv. Photonics **1**, 016001 (2019).
[45] Y. A. Nenasheva, Ceramic materials for high-quality dielectric resonators of microwave range, MRS Online Proceedings Library Archive **269**, 607 (1992).
[46] C. Larsson, C. Sohl, M. Gustafsson, and G. Kristensson, in *Nordic Radio Science and Communication Conference, 2008* (Lund University Press, Växjö, 2008).
[47] R. De Porrata-Doria i Yague, A. Ibars, and L. Martinez, Analysis and reduction of the distortions induced by time-domain filtering techniques in network analyzers, IEEE Trans. Instrum. Meas. **47**, 930 (1998).
[48] C. Larsson and M. Gustafsson, Wideband measurements of the forward RCS and the extinction cross section, ACES Journal **28**, 8 (2013).
[49] M. Odit, K. Koshelev, S. Gladyshev, K. Ladutenko, Y. Kivshar, and A. Bogdanov, Observation of supercavity modes in subwavelength dielectric resonators, Adv. Mater. **33**, 2003804 (2021).
[50] A. Gelessus, W. Thiel, and W. Weber, Multipoles and symmetry, J. Chem. Educ. **72**, 505 (1995).
[51] K. Ohtaka and Y. Tanabe, Photonic bands using vector spherical waves. III. Group-theoretical treatment, J. Phys. Soc. Jpn. **65**, 2670 (1996).
[52] S. Gladyshev, K. Frizyuk, and A. Bogdanov, Symmetry analysis and multipole classification of eigenmodes in electromagnetic resonators for engineering their optical properties, Phys. Rev. B **102**, 075103 (2020).
[53] E. L. Ivchenko and G. Pikus, *Superlattices and Other Heterostructures: Symmetry and Optical Phenomena*, Springer Series in Solid-State Sciences (Springer-Verlag, Berlin Heidelberg, 1995).
[54] J. Wiersig, Formation of Long-Lived, Scarlike Modes near Avoided Resonance Crossings in Optical Microcavities, Phys. Rev. Lett. **97**, 253901 (2006).
[55] M. V. Rybin, K. L. Koshelev, Z. F. Sadrieva, K. B. Samusev, A. A. Bogdanov, M. F. Limonov, and Y. S. Kivshar, High-Q Supercavity Modes in Subwavelength Dielectric Resonators, Phys. Rev. Lett. **119**, 243901 (2017).
[56] K. Koshelev, S. Kruk, E. Melik-Gaykazyan, J.-H. Choi, A. Bogdanov, H.-G. Park, and Y. Kivshar, Subwavelength dielectric resonators for nonlinear nanophotonics, Science **367**, 288 (2020).
[57] V. Mylnikov, S. T. Ha, Z. Pan, V. Valuckas, R. Paniagua-Dominguez, H. V. Demir, and A. I. Kuznetsov, Lasing action in single subwavelength particles supporting supercavity modes, ACS Nano (2020).
[58] J. D. Jackson, *Classical Electrodynamics* (Wiley, New York, 1998), 3rd ed.

[59] R. Alaee, C. Rockstuhl, and I. Fernandez-Corbaton, An electromagnetic multipole expansion beyond the long-wavelength approximation, Opt. Commun. **407**, 17 (2018).

[60] R. E. Noskov, I. I. Shishkin, H. Barhom, and P. Ginzburg, Non-mie optical resonances in anisotropic biomineral nanoparticles, Nanoscale **10**, 21031 (2018).

[61] H. Barhom, A. A. Machnev, R. E. Noskov, A. Goncharenko, E. A. Gurvitz, A. S. Timin, V. A. Shkoldin, S. V. Koniakhin, O. Y. Koval, M. V. Zyuzin, A. S. Shalin, I. I. Shishkin, and P. Ginzburg, Biological kerker effect boosts light collection efficiency in plants, Nano Lett. **19**, 7062 (2019).

[62] C. Eckart and G. Young, A principal axis transformation for non-hermitian matrices, Bull. Am. Math. Soc. **45**, 118 (1939).

[63] B. C. Brock, *Using vector spherical harmonics to compute antenna mutual impedance from measured or computed fields*, Tech. Rep. (Sandia National Labs., Albuquerque, NM, and Livermore, CA (US), 2000).

[64] J. L. Opsal and W. M. Visscher, Theory of elastic wave scattering: Applications of the method of optimal truncation, J. Appl. Phys. **58**, 1102 (1985).

[65] M. B. Doost, W. Langbein, and E. A. Muljarov, Resonant-state expansion applied to three-dimensional open optical systems, Phys. Rev. A **90**, 013834 (2014).

[66] P. Lalanne, W. Yan, K. Vynck, C. Sauvan, and J.-P. Hugonin, Light interaction with photonic and plasmonic resonances, Laser Photonics Rev. **12**, 1700113 (2018).

[67] F. Alpeggiani, N. Parappurath, E. Verhagen, and L. Kuipers, Quasinormal-Mode Expansion of the Scattering Matrix, Phys. Rev. X **7**, 021035 (2017).

[68] T. Weiss and E. A. Muljarov, How to calculate the pole expansion of the optical scattering matrix from the resonant states, Phys. Rev. B **98**, 085433 (2018).

[69] K. Koshelev and A. Bogdanov, in *AIP Conf. Proc.* (AIP Publishing LLC, New York, 2017), Vol. 1874 p. 030020.

[70] M. I. Mishchenko, J. W. Hovenier, and L. D. Travis, *Light Scattering by Nonspherical Particles* (Academic Press, San Diego, 2000).